Mon. Not. R. astr. Soc. (1988) **235**, 297–313

Giant H II regions as distance indicators – II. Application to H II galaxies and the value of the Hubble constant*

Jorge Melnick†‡ *European Southern Observatory, Karl Schwarzschild Str. 2, D-8046, Garching bei Munchen, FRG*

Roberto Terlevich†‡ *Royal Greenwich Observatory*

Mariano Moles†‡ *Instituto de Astrofísica de Andalucia*

Accepted 1988 March 22. Received 1988 February 26; in original form 1987 April 28

Summary. The (integrated) Hβ luminosities of giant H II regions and of H II galaxies (giant H II regions in dwarf galaxies) can be predicted with an accuracy comparable to the observational errors from the velocity widths of their emission-line profiles and the nebular oxygen abundances. The zero point of the correlation between these parameters is calibrated using the homogeneous sample of giant H II regions in nearby galaxies with well determined distances discussed in the first paper of this series. The calibration is applied to distant H II galaxies to obtain a value for Hubble's constant H_0. After correcting the fluxes for Malmquist bias and the radial velocities for the motion of the Local Group we find $H_0=89\pm10\,\mathrm{km\,s^{-1}\,Mpc^{-1}}$. From four H II galaxies in the Virgo cluster, a true distance modulus of $(m-M)_{\mathrm{vir}}=30.9\pm0.15$ is obtained for that cluster. The effects of the large-scale inhomogeneities in the Hubble flow shown to exist by Dressler *et al.* are emphasized and illustrated using the distance to Virgo to calibrate the kinematical distances of six rich clusters out to redshifts of $\sim 9000\,\mathrm{km\,s^{-1}}$. We conclude that values of H_0 obtained using 'nearby' ($cz<5000\,\mathrm{km\,s^{-1}}$) galaxies may be systematically biased by streaming motions. A detailed discussion of possible systematic errors is presented.

1 Introduction

1.1 H II REGIONS AS DISTANCE INDICATORS

In the first paper of this series (Melnick *et al.* 1987, Paper I) we showed that the correlations between global parameters of giant H II regions can be used as distance indicators. In particular,

*Partly based on observations obtained at the European Southern Observatory, La Silla, Chile.
†Visiting astronomer, Cerro Tololo Interamerican Observatory operated by AURA Inc. under contract with the National Science Foundation of the USA.
‡Guest investigator, Mount Wilson and Las Campanas Observatories, Carnegie Institution of Washington.

we showed that the reddening corrected Hβ luminosities of giant H II regions, $L(\mathrm{H}\beta)$, are well correlated with σ, the rms velocity width of the emission-line profiles. We also showed that the scatter in the relation between $L(\mathrm{H}\beta)$ and σ is correlated with the oxygen abundance of the nebular gas (O/H), and we used Principal Component Analysis (PCA) techniques to show that the Hβ luminosities of young H II regions are determined by the parameter $M_z = R_c\sigma^2/(\mathrm{O/H})$ which is thus a good distance indicator for giant H II regions (R_c is the nebular core radius).

In order to apply these results to determine the value of Hubble's constant, H_0, it is imperative to observe galaxies whose recession velocities are not affected by local mass concentrations and (if that were possible) by large-scale streaming motions. This requires observations of galaxies outside the Local Supercluster and, ideally, beyond 50–60 Mpc.

The brightest H II regions found in the most luminous spirals reach Hβ luminosities of $10^{40}\,\mathrm{erg\,s^{-1}}$ and linear diameters of a few hundred parsec. If located at the edge of the Local Supercluster, these H II regions would have an apparent flux of only a few times $10^{-14}\,\mathrm{erg\,s^{-1}\,cm^{-2}}$ and angular diameters of 2–3 arcsec. Thus, using H II regions in bright distant spirals is clearly a tortuous path towards the Hubble constant.

1.2 H II GALAXIES

Haro (1956), Zwicky (1966), Markarian (1967) and Sargent & Searle (1970), among others, have identified a new class of galaxies (known as blue compact or *H II galaxies*) characterized by having

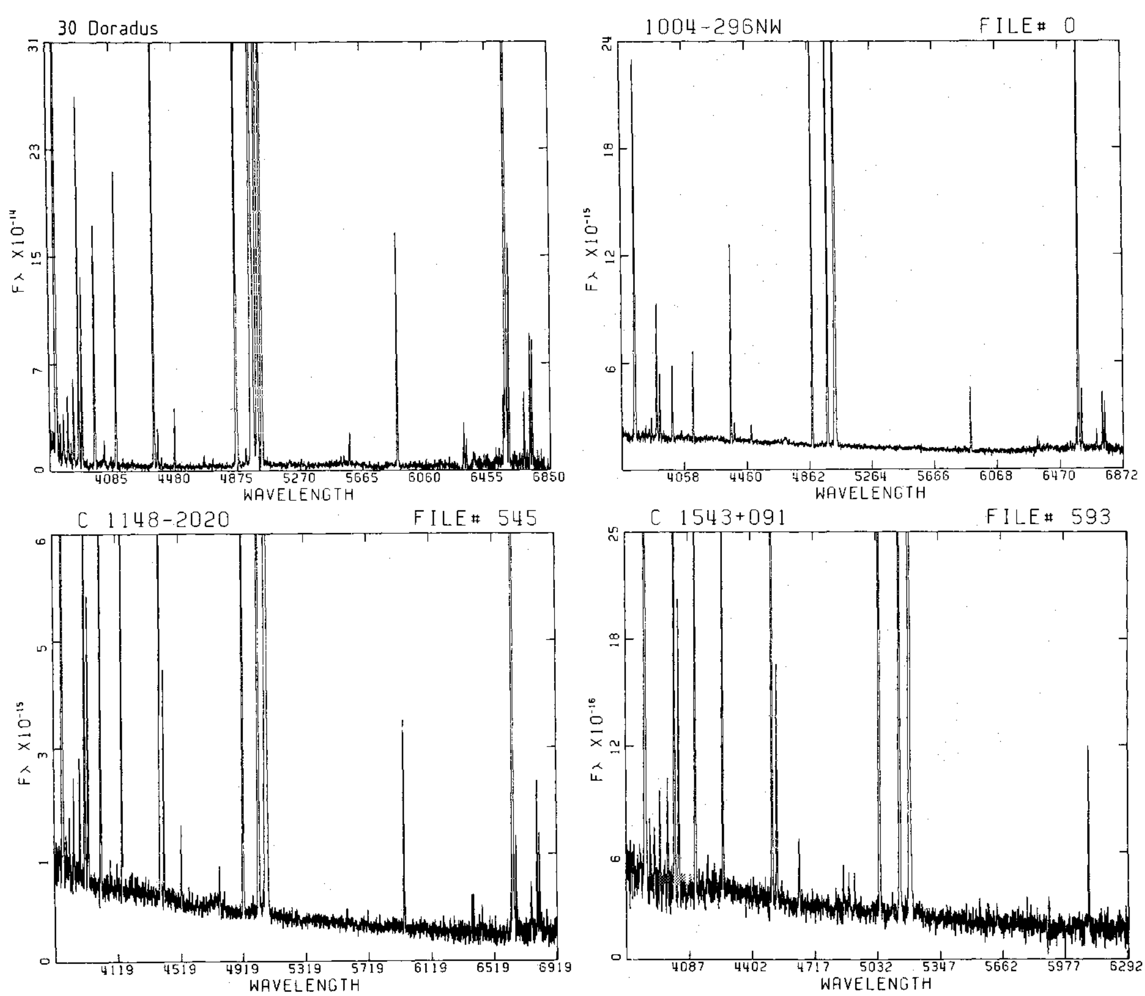

Figure 1. Spectra of three representative H II galaxies and of the prototype giant H II region 30 Doradus.

small dimensions, spheroidal shapes, very young stellar populations and spectral properties *indistinguishable* from those of low-abundance giant extragalactic H II regions. This is illustrated in Fig. 1 where spectra of three representative H II galaxies are compared with the spectrum of the proto-typical giant H II region 30 Doradus (LMC).

H II galaxies are frequently found in objective prism surveys; about 20 per cent of the emission line galaxies in the Tololo (Smith, Aguirre & Zelman 1976) and Michigan (McAlpine & Williams 1981) surveys belong to this type. In most cases H II galaxies are associated with low surface brightness amorphous galaxies, probably Magellanic type irregulars (Melnick, Terlevich & Eggleton 1985; Campbell, Terlevich & Melnick 1986). However, the presence of an old underlying component is not evident in all H II galaxies and in fact a significant fraction are compact with no evidence for extension, indicating that they may be truly intergalactic giant H II regions (Melnick 1987). Giant H II regions also tend to be associated with low surface brightness regions of galaxies. For example NGC 5471, the largest H II region in the giant Sc galaxy M101, was for a long time considered to be a companion to that galaxy and not a giant H II region (Seyfert 1940).

The only important spectral difference between H II galaxies and the giant H II regions discussed in Paper I is that the former are systematically metal poorer. This difference is mostly a reflection of the relationship between abundance and mass for late type galaxies (Skillman *et al.* 1988) but is also partly due to a selection effect; for abundances larger than that of the Orion nebula [$12+\log(O/H) \sim 8.5$] it is extremely difficult to obtain accurate abundances.

The close similarities between giant H II regions in late-type galaxies and H II galaxies strongly suggest that the methods discussed in Paper I for deriving distances to giant H II regions can be applied to H II galaxies and thus extended to much larger distances. In this paper we present a detailed study of the global properties of a sample of H II galaxies selected from the *Spectrophotometric Catalogue of H II Galaxies* (Terlevich *et al.*, in preparation). We show that H II galaxies exhibit correlations which are very similar to those observed in giant H II regions and we combine the two classes to derive a value of the Hubble constant.

2 Observations

2.1 SELECTION OF THE SAMPLE

The *Spectrophotometric Catalogue of H II Galaxies* (Terlevich *et al.*, in preparation, henceforth the SCHG) contains data for more than 400 objects selected from objective prism surveys mostly of the southern hemisphere. We have selected about 100 H II galaxies for high S/N spectrophotometric studies, aimed at determining reliable elemental abundances, and for line-profile studies of the kinematics of the ionized gas.

The objects were chosen primarily on the basis of their Hβ fluxes (secondary criteria included position in the sky and equivalent width of Hβ) using as a starting point low dispersion spectrophotometry obtained with the IDS scanner at the 3.6-m telescope at La Silla. Thus, our sample is magnitude limited although it does not comprise all the brightest galaxies in the SCHG which, in any case, is not complete in any well-defined statistical sense. The sample for which we have line profile information, henceforth the 'echelle' sample, comprises 49 galaxies brighter than $F(\mathrm{H}\beta)=5\times10^{-15}$ erg s^{-1} cm^{-2} and with Hβ equivalent widths, $W(\mathrm{H}\beta)$, larger than 30 Å. This restriction is necessary to limit the sample to young nebulae in order to minimize evolutionary effects (Copetti, Pastoriza & Dottori 1986). Although, in principle, age effects can be explicitly considered because $W(\mathrm{H}\beta)$ is a reliable age indicator for giant H II regions (Copetti *et al.* 1986, and references therein), in practice the continua of H II galaxies are influenced to varying extents by the background stellar population of the parent galaxies and therefore $W(\mathrm{H}\beta)$ is not a reliable age indicator for all H II galaxies.

Table 1. The echelle sample

SCHG	*Other names*	*Z*	σ $km\ s^{-1}$	$\delta\sigma$	$F(H_\beta)$ $10^{-13} erg\ s^{-1}$	$C(H_\beta)$	$W(H_\beta)$ Å	12+ $log(O/H)$	REFERENCES
0105-387	T0104-388	0.021	49.0	0.0	0.3:	0.39	50		1,B
0127-397	T0127-397	0.016	33.7	0.7	0.50	0.51	40		1,A,B
0131+007	MICH 336	0.020	16.7	0.5	0.08	0.06	40		2,B
0142+046	MICH 133	0.009	17.2	0.0	0.32	0.43	65		2,B
0226-390	T0226-390	0.048	89.9	3.5	0.57	0.56	90		1,A,B
0242-387	T0242-387	0.126	134.0	5.0	0.22	0.79	60	8.23	1,A,B
0341-407E	C341-4045	0.015	22.0	1.5	0.44	0.28	140	8.04	3,A,B
0341-407W	C341-4045	0.015	23.0	1.5	0.23	0.32	40		3,A,B
0357-392	C357-3915	0.074	51.1	0.6	0.47	0.17	180	7.87	3,A,B
0440-381	T0440-381	0.041	39.7	1.5	0.3:	0.32	35	8.31	1.A,B
0513-393	T0513-393	0.050	33.2	3.0	0.18	0.29	145	7.90	1,A,B
0553+036	IIZW40	0.003	35.2	0.5	1.9:	1.00	170	8.13	6,B
0633-415	T0633-415	0.018	31.8	1.0	0.45	0.35	90	8.09	1,A,B
0645-376	T0645-376	0.026	32.1	1.0	0.20	0.52	50	8.19	1,A,B
0839+120	C0840+1201	0.030	36.5	0.7	0.48	0.52	105	7.88	3,A
0839+107	C0840+1044	0.012	34.0	0.5	0.1:	0.39	55		3,B
0842+162	C08-28A	0.054	49.1	2.5	0.28	0.77	35		3,A,B
1004-294S	T1004-294	0.004	30.6	0.5	2.70	0.69	60	8.23	1,A,B
1004-294N	T1004-294	0.004	32.3	0.5	3.10	0.77	60	8.28	1,A,B
1008-287	T1008-286	0.014	24.0	1.7	0.30	0.52	125	8.16	1,A,B
1025-284	T1025-284	0.032	25.2	1.0	0.30	0.48	60	8.06	1,A,B
1042+096	FAIRALL 2	0.056	38.8	1.0	0.27	0.40	100	8.11	4,A
1053+064	FAIRALL 30	0.004	21.8	0.5	1.80	0.22	90	8.01	4,A
1102+294	MARK 36	0.002	16.0	1.0	1.4:	0.7:	70	7.86	5,A
1116-326	T1116-325	0.002	12.0	1.0	0.43	0.43	275	8.31	1,A
1134+010E	MICH 439E	0.004	19.7	0.5	0.48	0.60	60	8.05	2,A
1139+006	MICH 448	0.018	40.8	0.5	2.20	0.79	45		2,A
1147-283	T1147-283	0.006	18.9	0.5	0.24	0.47	45	7.90	1,A
1147+002	MICH 455	0.012	20.6	0.5	0.09	0.26	55	7.84	2,B
1148-020	MICH 461A	0.005	14.5	0.5	0.70	0.40	155	7.74	2,A
1148-203	C1148-2020	0.012	33.3	1.0	1.80	0.30	230	8.01	3,A
1150-021A	MICH 462A	0.003	18.5	0.5	0.75	0.38	75	7.98	2,A
1150-021B	MICH 462B	0.003	18.9	1.0	1.30	0.38	90	7.79	2,A
1158+130	C12-39	0.067	84.5	2.5	0.24	4.88	200	8.20	3,A
1210+119		0.023	34.2	1.5	0.13	0.63	60		7,A
1210+110		-0.001	18.5	1.0	0.2:	0.30	110		7,A
1214-277	T1214-277	0.026	27.6	2.0	0.30	0.29	230	7.58	1,B
1304-386	T1304-386	0.014	33.8	0.5	0.59	0.46	300	7.98	1,A
1324-276	T1324-276	0.006	33.4	1.0	0.87	0.35	115	8.20	1,A
1334-326	T1334-326	0.013	16.4	0.0	0.3:	0.22	265		1,A
1345-421	T1345-420	0.008	21.6	0.5	0.38	0.26	70	8.07	1,A
1405-177	C1406-1742	0.034	23.9	0.0	0.10	0.36	50		3,A
1409+119	C1409+1200	0.056	52.3	0.5	0.19	0.44	130	8.18	3,A
1457-262A	T1457-262	0.018	51.5	1.0	2.10	0.70	95	8.19	1,A

Table 1 – *continued*

SCHG	*Other names*	*Z*	σ $km\ s^{-1}$	$\delta\sigma$	$F(H_\beta)$ $10^{-13} erg\ s^{-1}$	$C(H_\beta)$	$W(H_\beta)$ Å	12+ $log(O/H)$	REFERENCES
1457-262C	T1457-262	0.018	26.3	0.5	0.18	0.79	40		1,A
1543+091	C1543+0907	0.038	34.6	2.5	0.54	0.31	240	7.79	3,A
1924-416	T1924-416	0.009	29.9	0.5	3.83	0.17	100	7.90	1,B
2138-405	T2138-405	0.058	55.5	2.5	0.33	0.25	120		1,B
2326-405	T2326-405	0.051	34.5	0.5	0.14	0.22	80	8.03	1,B

References

Surveys

1. Tololo survey (Smith, Aguirre & Zemelman, 1976; Smith, private communication).
2. Michigan survey (McAlpine & Williams 1981).
3. Cambridge survey (Hazard 1985, and references therein).
4. Fairall (1980).
5. Markarian, Lipovetskii & Stepanian (1981).
6. Zwicky (1971).
7. SCHG.

Photometry

A. SCHG.
B. This paper.

Table 1 lists the relevant data of the echelle sample including the identification in the SCHG and references to their discovery catalogues. Accurate positions and finding charts may be found in these references.

2.2 TOTAL OXGEN ABUNDANCES (O/H)

The oxygen abundances have been taken from the SCHG. Most abundances have been calculated using spectrophotometry obtained with the Reticon scanner of the 2.5-m DuPont telescope at Las Campanas; a few values were obtained using IDS spectrophotometry from La Silla. Abundances for 34 galaxies in the echelle sample are thus available. Details of the spectrophotometric observations, reduction procedures and methods employed to calculate abundances have been given in the papers by Campbell *et al.* (1986) and Pagel, Terlevich & Melnick (1986) to which we refer for further details. From repeated observations and from signal-to-noise statistics we estimate the mean accuracy in O/H to be $\delta \log(O/H)=0.15$.

2.3 Hβ LUMINOSITIES

Fluxes, $F(H\beta)$, extinction coefficients, $C(H\beta)$, and distances are required to derive Hβ luminosities. We will discuss the first two items here and consider the determination of distances separately below. Hβ fluxes for the echelle sample come primarily from the SCHG. However, not all the observations of that catalogue were obtained under 'photometric' conditions; because of either poor weather or the use of small entrance apertures, about 50 per cent of the absolute Hβ fluxes given in the SCHG have uncertainties of 20 per cent or larger so only 32 of the 49 galaxies in the echelle sample have accurate integrated Hβ fluxes in the SCHG.

We obtained additional photometry using the Boller and Chivens spectrograph of the 2.2-m telescope at La Silla on 1986 December 6 and 7. The spectra were recorded with a cooled RCA SID501 320×512 CCD and cover a spectral range of about 3000 Å centred at 5500 Å. The weather conditions were photometric and we used a long, 6 arcsec wide, entrance slit, in order to obtain the integrated spectrum (the seeing on both nights was better than 1 arcsec). A minimum of eight standard stars were observed each night to ensure photometric reductions. The reductions, including bias and flat field corrections, and standard calibrations were done using the IHAP package at ESO Garching. From these data we extracted Hβ fluxes and Balmer decrements which are presented in Table 1. In the cases where we had previous IDS photometry, the results presented in Table 1 are averages. From these averages and/or from the internal consistency of the instrumental response curves obtained from different standard stars we estimate the Hβ fluxes to be accurate to better than 10 per cent and the Balmer decrements to be accurate to 5 per cent or better. In total we have accurate fluxes for 42 galaxies in the echelle sample.

2.4 EMISSION-LINE PROFILE WIDTHS

Echelle observations of H II galaxies were carried out in five observing runs between 1981 January and 1983 May using the echelle spectrograph of the 4-m telescope at Cerro Tololo. The spectra were recorded using blue sensitive Vidicon television detectors and covered different spectral ranges. Exposure times ranged from 15 min to 2 h. A typical H II galaxy spectrum is reproduced in Plate 1 which shows a Versatec copy of a full Vidicon frame of the double galaxy SCHG 1150-021 (Mich 462).

An important instrumental effect that needs to be discussed in the present context is beam bending. This is a distortion of the instrumental profile due to the deflection of the TV-reading beam in regions of high surface density of charge on the silicon target. Thus, beam-bending affects mostly the cores of strong, narrow emission lines. We have not attempted to correct our profiles for this effect; we have merely discarded lines with peak fluxes stronger than the minimum levels at which we detected significant distortions in the lines of the thorium–argon calibration spectrum. In practice, this meant that in the majority of cases the [O III] λ5007 line could not be used.

The data were reduced in a straightforward manner using the VAX computers at ESO, Garching. The spectra along each echelle order were extracted using the MIDAS/Caspec package and the resulting one-dimensional spectra were measured using the line analysis package ALICE. ALICE fits the continua with polynomials and the line profiles with single Gaussians. The resulting widths in pixels were transformed to wavelength units using equations obtained from the comparison spectrum. The resulting velocity dispersions, corrected for thermal and instrumental broadening, $\sigma_0^2=\sigma_{obs}^2-\sigma_{th}^2-\sigma_{inst}^2$, are presented in Table 1 together with estimates of their uncertainties. The uncertainties were assessed either from multiple observations or from the internal consistency of several lines. The width of the instrumental profile was obtained from unsaturated thorium lines and was typically 2.2 pixels, corresponding to 0.44 Å *FWHM* at Hβ $\sigma_{inst}=11.5\ \mathrm{km\,s^{-1}}$. This varied slightly with the different instrumental configurations we used. The corrections for thermal broadening were obtained assuming a constant electron temperature of $T_e=10\,000$ K for all objects. This does not introduce any serious systematic effect since the widths were mostly derived from the [O III] λ4959 lines which are only marginally affected by thermal broadening. Fig. 2 presents representative profiles for six objects covering the full range of line profile widths of our sample. The figure also shows the spectrum of a strong but unsaturated thorium line. Because of beam-bending the line is broadened to 3.3 pixels and shows a small bump in the blue wing. The similar bumps present in the wings of some (especially the narrow line) H II galaxies are due to this effect. The Gaussian fits used to derive the linewidths

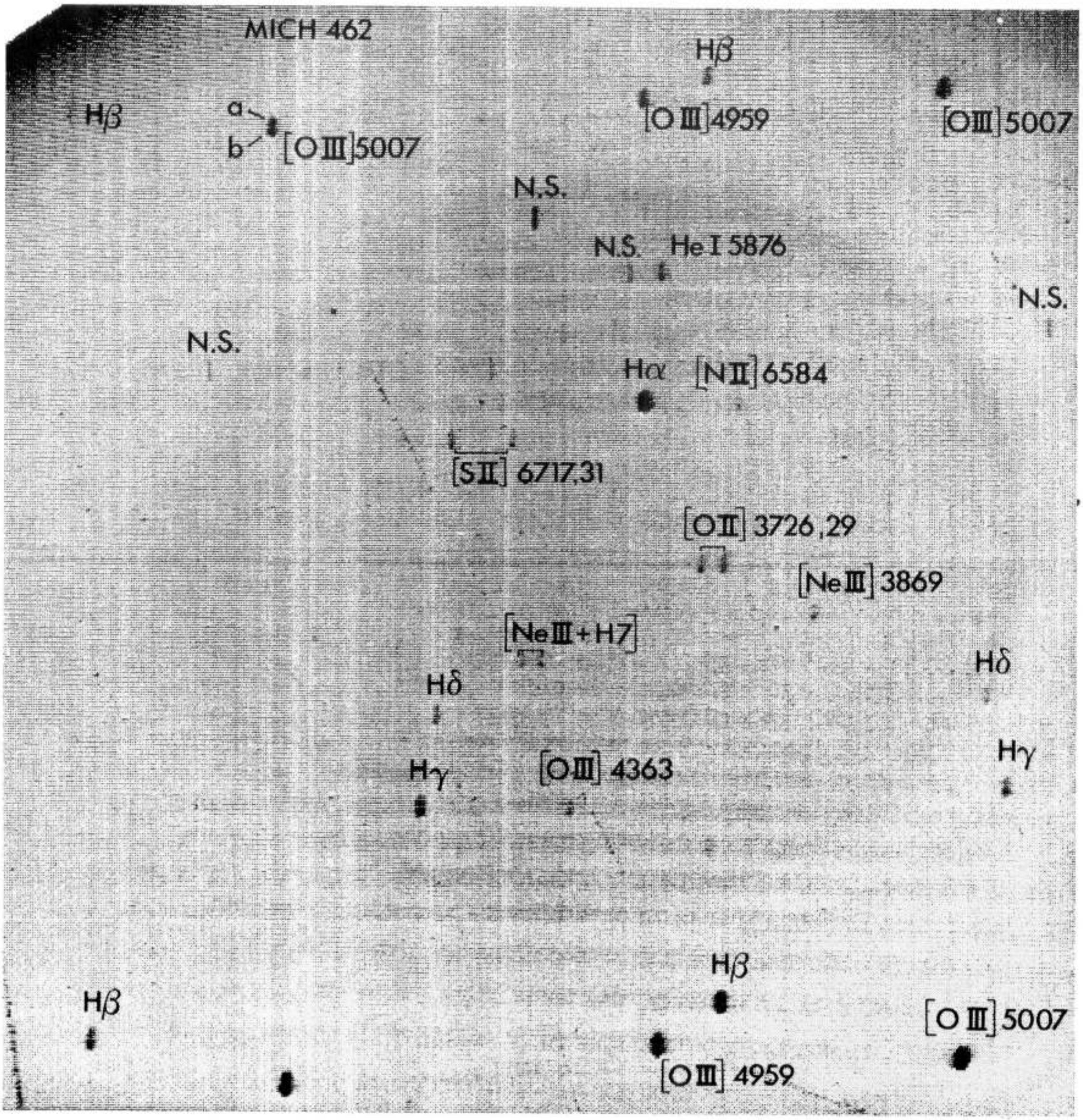

Plate 1. Versatec print of the full echelle spectrum of the double H II galaxy SCHG 1150−021=Michigan 462. The spectrum covers two orders of the cross-disperser so that the green lines (Hβ and [O III]) appear twice. A BG-38 filter was used to separate both orders and this explains the fading of the orders in the central (blue) part.

[*facing page* 302]

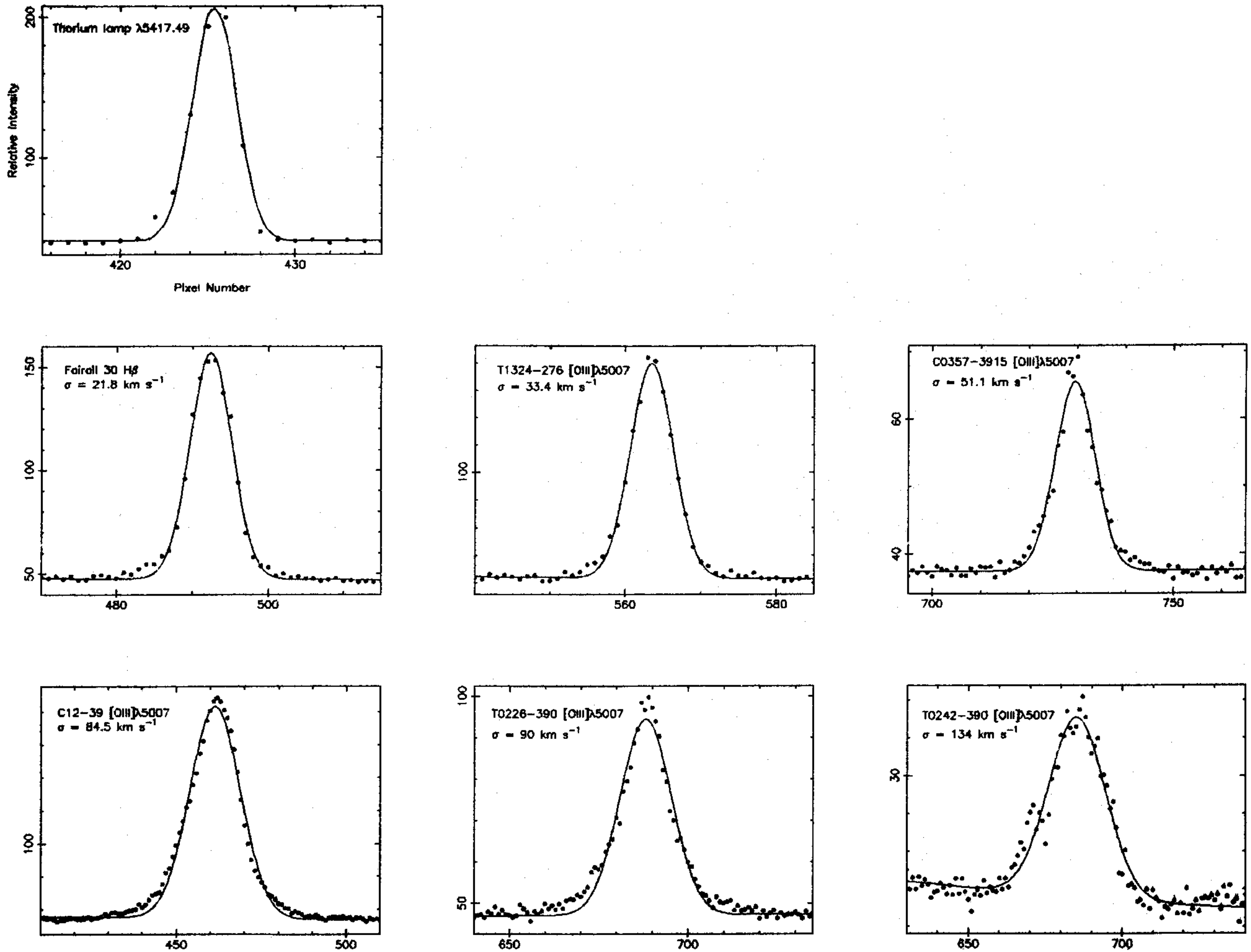

Figure 2. Emission line profiles of six H II galaxies covering the full range of profile widths present in the echelle sample. The wavelength scale is in pixels. Also shown are the Gaussian fits used to derive the velocity widths of the profiles which are given in the upper-left side of each pilot.

are shown in this figure. Notice that in some cases, in particular in the galaxies with the broadest lines, the observed profiles are not well represented by single Gaussians.

2.5 RADIAL VELOCITIES AND DISTANCES

It is very easy to get accurate radial velocities for H II galaxies: their strong, narrow emission lines can be adequately detected in exposures of only a few seconds. Our redshifts are accurate to a few tens of $km\,s^{-1}$, but the observed radial velocities must be corrected by several effects before they can be used to infer the distances of the objects, and these corrections are somewhat uncertain. We have applied the standard IAU correction for the motion of the Sun relative to the Local Group. This correction does not include the motion of the Galaxy in the Local Group (Yahil, Sandage & Tammann 1977; Sandage 1986) and this may introduce uncertainties of several tens of $km\,s^{-1}$ in the radial velocities.

Two additional corrections must be applied: infall into the Virgo cluster (of the galaxy as well as of some of the programme objects) and large-scale streaming motions (as inferred from the dipole anisotropy of the Cosmic Microwave Background, CMWB). We have closely followed the precepts of Aaronson *et al.* (1982) together with their case 6 solution (0, 0, 300:1080; Aaronson *et al.* 1986) to correct the radial velocities for the influence of the Virgo cluster, and we have assumed a kinematical distance of 1080 $km\,s^{-1}$ for the five H II galaxies in the echelle sample which are at the redshift and position of the Virgo cluster.

The removal of large-scale streaming motions poses a severe problem. The simplest interpretation of the dipole anisotropy of the CMWB is that the Local Group moves, with respect to the CMWB, with a velocity of 614 $km\,s^{-1}$ towards $l=269$, $b=28$ (Lubin *et al.* 1985), roughly in the direction of the Hydra–Centaurus supercluster (Tammann & Sandage 1985; Dressler *et al.* 1987). Thus, in principle, we should remove the corresponding projection of this velocity from our objects if they are at rest with respect to the CMWB. Galaxies closer than $cz{\sim}6000\,km\,s^{-1}$, however, appear to have significant peculiar velocities, particularly those lying in the direction of the CMWB dipole (Dressler *et al.* 1987). Therefore we have not *a priori* corrected our velocities for the motion of the Sun relative to the CMWB but we will consider this effect explicitly in the discussion of our result for the Hubble constant (Section 5).

3 Data analysis

In order to construct a distance indicator using giant H II regions and H II galaxies we must be sure that their global properties are the same. Specifically, we must ascertain that the integrated Hβ luminosities of H II galaxies depend only upon their velocity dispersions, core radii and metallicities, and that the dependence has the the same functional form as the one found in Paper I for giant H II regions. In this section we will apply the analysis of Paper I to the echelle sample. An important difference will be that for H II galaxies we do not have core radii. As we shall see, however, it turns out that velocity dispersion and oxygen abundance suffice to completely determine (within the observational errors) the luminosities of H II galaxies, a result not unexpected since for giant H II regions the radii are correlated with the velocity dispersions.

3.1 CORRELATIONS

Fig. 3 presents a logarithmic plot of $L(H\beta)$ (assuming a Hubble constant of $H_0=100\,km\,s^{-1}\,Mpc^{-1}$ to compute the distances) as a function of velocity dispersion σ corrected for redshift $\sigma=\sigma_0/(1+z)$. Also plotted are the giant H II regions from Paper I. The solid line presents the regression line for the giant H II region data alone. There are two features of this plot which we

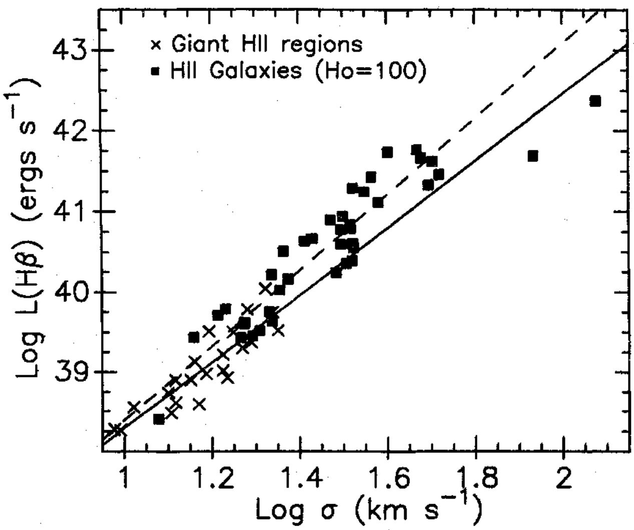

Figure 3. Logarithmic plot of the integrated Hβ luminosities of giant H II regions and H II galaxies versus the rms widths of their emission line profiles. The solid line shows a least squares fit to the giant H II regions data and the dashed line the corresponding fit to the H II galaxies. A Hubble constant of H_0=100 km s^{-1} Mpc^{-1} was used to compute the H II galaxies' luminosities.

would like to discuss here. The first is that, even with H_0=100, most H II galaxies lie *above* the regression line for giant H II regions. We will show below that this is an effect of metallicity: on average the H II galaxies in our sample are a factor of 1.6 oxygen poorer than the giant H II regions of Paper I. Thus, for a given velocity dispersion, H II galaxies are on average a factor of 1.5 brighter than giant H II regions (see below).

The second feature of Fig. 3 we must worry about is that two H II galaxies lie below the giant H II region line. The discrepancy is not a metallicity effect; both galaxies are relatively metal rich but not enough to explain their location in the [$\log L(\mathrm{H}\beta), \log\sigma$] plane. Therefore, either a significant fraction of the line-broadening in these two galaxies is independent of the Hβ luminosity (and hence of the ionizing source) or the $\log L(\mathrm{H}\beta) - \log\sigma$ relation is curved. The two galaxies are at large redshifts and therefore are difficult to resolve even on deep CCD pictures but, while 0226−390 is unresolved, 0242−387 is clearly double and appears to be in the centre of a distant cluster. In fact the emission line profiles of this galaxy have two distinct components (*cf.* Fig. 2). The results of Paper I can be used to show that *single* giant H II regions with lines broader than ~60 km s^{-1} cannot exist. This is so because the sizes of the ionizing clusters of giant H II regions cannot be so large that their dynamical time-scales are longer than the main-sequence lifetimes of the ionizing stars. Otherwise one would not expect a correlation between Hβ luminosity and velocity dispersion. Since the radii of the ionizing clusters correlate with velocity dispersion (Paper I), the existence of a limiting radius implies a maximal value of σ. Therefore, in what follows, we will restrict the analysis to H II galaxies with lines narrower than σ=60 km s^{-1}. We should keep in mind, however, that to some extent, the profiles of all H II galaxies may be affected by the gravity of an underlying old stellar component so that we must consider the effect of curvature of the [$\log L(\mathrm{H}\beta)$,$\log\ \sigma$] relation in the final analysis of the results.

The dashed line in Fig. 3 shows the least-squares fit for the H II galaxies alone. The parameters of that line are given by,

$$\log L(\mathrm{H}\beta) = (4.70\pm0.30)\log\sigma + 33.61\pm0.50.$$

The rms scatter is $\delta \log L(\mathrm{H}\beta)$=0.29. For comparison, the slope of the [$L(\mathrm{H}\beta), \sigma$] correlation for giant H II regions (Paper I) is 4.17±0.47 with an rms scatter $\delta \log L(\mathrm{H}\beta)$=0.22. From Paper I we

Table 2. Principal component analysis

	Eigenvectors					
	HII Galaxies			Giant HII regions		
Parameter	1	2	3	1	2	3
$\log L(H_\beta)$	0.68	0.22	0.69	0.69	-0.18	0.70
$\log \sigma$	0.70	0.00	-0.71	0.71	-0.03	-0.71
log(O/H)	0.19	0.98	0.12	0.15	0.98	0.10
Eigenvalues	66%	33%	1%	64%	33%	3%

know that this scatter is correlated with the oxygen abundance of the giant H II regions. In order to test for this effect in H II galaxies, following Paper I, we will make use of Principal Component Analysis (PCA) techniques. Table 2 shows the result of the PCA table for the echelle sample in the $[L(\mathrm{H}\beta), \sigma, \mathrm{O/H}]$ parameter space. Unfortunately our PCA routine (Paper I) does not include error analysis but even without considering errors, the eigenvalues and eigenvectors of the principal components of H II galaxies are remarkably similar to those of giant H II regions, also shown in Table 2. The PCA table shows that for H II galaxies two principal components contain 99 per cent of the weight and therefore that the global Hβ luminosities of *young* H II galaxies [recall that we imposed the condition $W(\mathrm{H}\beta)>30$ Å] are, within observational errors, completely specified by the line-profile widths and the oxygen abundances. The functional form of this relation, obtained from a least-squares fit is,

$$\log L(\mathrm{H}\beta)=(5.15\pm0.27)\log\sigma-(0.85\pm0.23)\log(\mathrm{O/H})+\mathrm{const.} \quad (1)$$

with an rms scatter of $\delta\log L(\mathrm{H}\beta)=0.21$ for 29 objects. The corresponding equation for giant H II regions is (Paper I),

$$\log L(\mathrm{H}\beta)=(0.86\pm0.11)\log R_c\sigma^2-(0.65\pm0.33)\log(\mathrm{O/H})+\mathrm{const.}$$

with an rms scatter of $\delta\log L(\mathrm{H}\beta)=0.21$. In giant H II regions the core radius, R_c, appears in the PCA. Since, from Paper I, $R_c \propto \sigma^3$, the relations for giant H II regions and for H II galaxies are remarkably similar. In the case of giant H II regions, the PCA analysis gives more stable results using R_c and σ than only σ but the scatter in the $[L(\mathrm{H}\beta), R_c\sigma^2, \mathrm{O/H}]$ relation is the same as the scatter of the $[L(\mathrm{H}\beta), \sigma, \mathrm{O/H}]$ relation. Thus, the effect of introducing the core radius is to reduce the sensitivity of the results to observational errors and errors in the distances but not to remove an additional degree of freedom. This illustrates the dangers, discussed in Paper I, of using least-squares techniques when the independent variable is subject to errors.

We conclude that there are no intrinsic differences between young H II galaxies and giant H II regions, and that, within the errors, the global Hβ luminosities of both classes of objects are determined by their profile widths and oxygen abundances in the manner described by equation (1). The relations $L(\mathrm{H}\beta) \propto \sigma^5$ and $R_c \propto \sigma^3$ (for giant H II regions) support the self-gravitating, variable IMF model proposed by Terlevich & Melnick (1981, *cf.* Paper I and references therein) to explain these correlations.

4 The distance indicator

The luminosities of H II galaxies can be predicted, with accuracies consistent with the observational errors, from their velocity dispersions and metallicities, which are independent of distance.

From the results of the previous section, the luminosities and therefore the distances of H II galaxies can be obtained using the parameter.

$$M_z = \frac{\sigma^5}{(\mathrm{O/H})}$$

which we shall call our 'distance indicator'. We have approximated the coefficients given by equation (1) to values consistent with their statistical errors. Fig. 4 shows a plot of $L(\mathrm{H}\beta)$ versus M_z for the 29 H II galaxies in the echelle sample that have accurate metallicities. The solid line shows a least squares fit to the data. The slope of this line is 1.03±0.05 and the rms scatter is $\delta \log L(\mathrm{H}\beta)=0.217$, only slightly larger than the scatter from equation (1). The dotted line in Fig. 4 shows a maximum likelihood fit to the data taking into account the observational uncertainties in both axes. The slope of this line is 1.07±0.04.

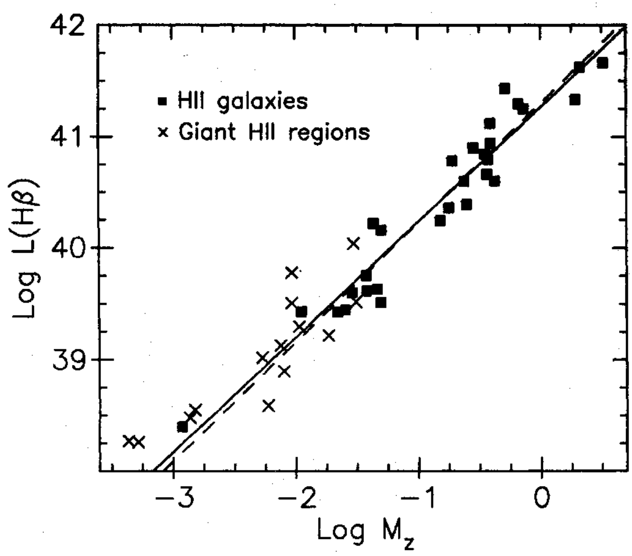

Figure 4. Logarithmic plot of Hβ luminosity versus the distance indicator parameter $M_z=\sigma^5/(\mathrm{O/H})$. The solid line shows a least-squares fit to the data and the dashed line shows a maximum-likelihood fit taking the errors in both axes into account. $H_0=100\,\mathrm{km\,s^{-1}\,Mpc^{-1}}$ was used to compute the luminosities.

Because the slopes determined using H II galaxies may, at least in principle, be affected by Malmquist bias, ideally both the zero point and the slope of the distance indicator should be determined using giant H II regions. In practice, however, as discussed in Section 3, the slope one determines for the 14 giant H II regions is very sensitive to the observational errors. For the data of Paper I using least-squares fitting techniques we obtain a slope of 0.83±0.13 while maximum-likelihood methods (which take the errors in both coordinates into account, Paper I) give a value of 1.02±0.08. Therefore, the 'true' slope of the correlation for giant H II regions is not significantly different from the value we find for H II galaxies. If we correct the luminosities of H II galaxies for Malmquist bias as described below, we obtain a maximum-likelihood slope of 0.99±0.04, consistent with the value determined for giant H II regions. Consequently, we have fixed the slope of the correlation to 1.0, and used this value to obtain the zero point from the giant H II regions. Thus, the 'complete' distance indicator has the functional form

$$\log L(\mathrm{H}\beta)=(1.0\pm0.04)\log M_z+(41.32\pm0.08). \quad (2)$$

We recall from Paper I that we have used the local distance scale of Aaronson *et al.* (1986) to compute the Hβ luminosities of giant H II regions. If we use the Sandage & Tammann (1974,

Table 3. Distance modulii to the zero point calibrators.

Galaxy	ST74	TA87	Here
LMC	18.59	18.50	18.50
SMC	19.27	18.85	18.89
NGC 6822	23.95	23.4	23.3
M33	24.56	24.4	24.17
NGC 2366	27.56	27.8	27.5
NGC 2403	27.56	27.8	27.5
Holmberg II	27.56	27.8	27.5
IC 2574	27.56	27.8	27.5
NGC 4236	27.56	27.8	27.5
M101	29.2	29.2	29.2

ST74) distance scale we obtain a zero point of 41.40±0.009 and if we adopt the new Sandage & Tammann local scale (Tammann 1987; TA87) we obtain 41.39±0.07. We note that the residuals are minimal for the TA87 scale [$\delta \log L(\mathrm{H}\beta)=0.255$ compared with 0.271 for our adopted scale and 0.324 for ST74]. For completeness, we present in Table 3 the list of the galaxies used in the calibration of the zero point, together with the relevant distance moduli.

5 The distance to H II galaxies

Before applying equation (2) to infer distances to H II galaxies it is necessary to consider the effect of Malmquist bias. Malmquist bias affects the $[L(\mathrm{H}\beta), M_z]$ correlation in exactly the same way it influences the Tully–Fisher relation and this has been extensively studied in the literature (Teerikorpii 1984; Bottinelli *et al.* 1986; Giraud 1987).

Giraud's formulation provides a quantitative way of correcting the observed luminosities for Malmquist bias as a function of the limiting flux of the sample, the precision of the distance indicator, and the mean and width of the luminosity function of H II galaxies in a bias free zone. Fig. 6 presents the luminosity function for ~200 galaxies in the SCHG that satisfy the condition $W(\mathrm{H}\beta)>30$ Å required to minimize age effects (*cf.* Section 2.1). The dashed line presents the luminosity distribution for galaxies within $750<cz<7500\,\mathrm{km\,s^{-1}}$, and the shaded area the luminosity distribution of the galaxies in the echelle sample. The main cause of Malmquist bias is clearly visible in Fig. 5 where most high luminosity objects appear at large redshifts. About 20 per cent of the high luminosity galaxies, however, have redshifts smaller than $cz=7500\,\mathrm{km\,s^{-1}}$ and most of these are in the echelle sample. In fact the galaxies in the echelle sample were selected among the brightest in the SCHG (the mean flux of the echelle sample is almost one order of magnitude brighter than that of the whole SCHG) in order to measure linewidths and oxygen abundances accurately. Thus, about 70 per cent of the H II galaxies in the echelle sample have radial velocities lower than $cz=7500\,\mathrm{km\,s^{-1}}$ and, *a priori*, therefore, our results should not be seriously affected by Malmquist bias. Indeed, using Giraud's (1987) equations assuming that the dashed curve in Fig. 5 is a good representation of the luminosity function of H II galaxies in the bias free zone we find that Malmquist bias leads us to overestimate the value of Hubble's constant by only ~10 per cent (Table 4).

5.1 THE HUBBLE CONSTANT

The luminosity distance of a given H II galaxy is given by the expression (Sandage 1975)

$$D_i^2=\frac{L_i(M_z)}{(1+z_i)^2 4\pi F_i(\mathrm{H}\beta)}$$

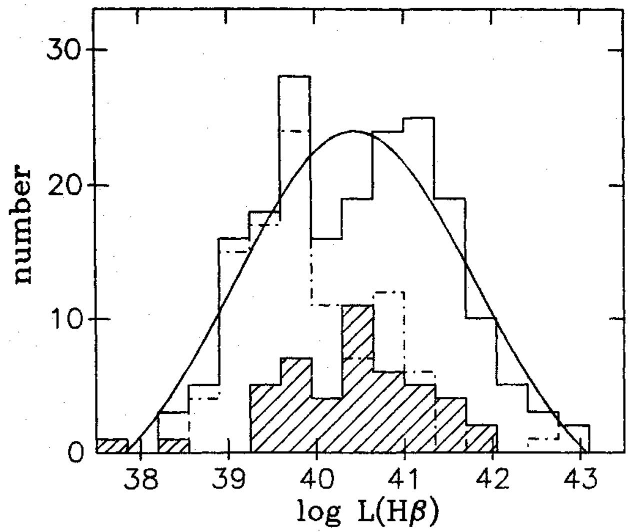

Figure 5. The solid line shows the luminosity function of all H II galaxies in the SCHG with $W(H\beta)>30$ Å. The dashed-dot line presents the luminosity function of H II galaxies within $750<cz<7500$ km s^{-1} and the shaded area shows the luminosity distribution of the galaxies in the echelle sample ($H_0=100$ km s^{-1} Mpc^{-1}).

Table 4. The Hubble constant.

redshift range	$< H_o >$ $km\ sec^{-1} Mpc^{-1}$	Malmquist correction	Corrected value	Number of objects
Full sample	94 ± 5	-11	83	29
Excluding Virgo	97 ± 5	-12	85	24
> 2000 $km\ sec^{-1}$	99 ± 5	-14	85	21
> 5000 $km\ sec^{-1}$	105 ± 7	-19	86	12

where $L_i(M_z)$ is the luminosity predicted by the distance indicator (equation 2), z_i is the redshift and $F_i(H\beta)$ is the observed flux corrected for extinction. The Hubble constant for an individual galaxy is then $H_i=V_i/D_i$ where V_i is the radial velocity corrected as described in Section 2.5. Mean values of H_0 are presented in Table 4 for different cuts of the echelle sample. Also included in that table are the standard deviations about these mean values and the corrections for Malmquist bias for each redshift range. Our bias-corrected estimate of $H_0=85\pm5$ km s^{-1} Mpc^{-1} compares very well with the value found by de Vaucouleurs and co-workers (de Vaucouleurs & Peters 1986, and references therein) and with $H_0=92$ km s^{-1} Mpc^{-1} derived by Aaronson *et al.* (1986) from the IR Tully–Fisher relation. Our result disagrees, however, with the value of $H_0=55\pm7$ preferred by Sandage and Tammann (Sandage 1984; Tammann 1987). Adopting their local distance scale does little to alleviate the discrepancy since the zero point difference corresponds to a change of only 8 per cent in distance. Because of the way our objects are distributed in the sky, the corrections for the motion of the Local Supercluster relative to the CMWB are mostly positive and therefore increase our estimate of the Hubble constant; assuming that H II galaxies beyond 5000 km s^{-1} are at rest relative to the CMWB and using the observed microwave dipole (Lubin *et al.* 1985; *cf.* Section 2.5) to correct our velocities, we get $H_0=89\pm6$ km s^{-1} Mpc^{-1}, to be compared with the value of 86±7 given in Table 4.

5.2 THE DISTANCE TO THE VIRGO CLUSTER

The distance to Virgo allows the calibration of the zero point of several distance indicators (Tammann 1987) and in particular of methods based on the properties of elliptical galaxies

(Dressler *et al.* 1987, and references therein). There are five H II galaxies in the echelle sample at the position and redshift of the Virgo cluster. From these we obtain a true distance modulus of $<(m-M)>=30.70\pm0.20$ to Virgo. However, the galaxy SCHG 1148−020 (Mich 461) has a modulus of only 30.0 so it may not be a member of the cluster. Excluding this galaxy we obtain a true distance modulus $(m-M)_{vir}=30.9\pm0.1$ to Virgo, which agrees with the value of $(m-M)_{vir}=30.82\pm0.12$ given by Aaronson *et al.* (1986) but which is significantly lower than the modulus of $(m-M)_{vir}=31.6\pm0.3$ favoured by Sandage and Tammann (TA87). In the following section we discuss possible systematic errors that may affect the giant H II region method and which eventually may have led us to overestimate the value of H_0. We consider, however, that our distance to Virgo is largely independent of systematic errors related to the extrapolation of the giant H II region relationships discussed above and in the next section, because the Hβ luminosities of the H II galaxies in the Virgo cluster are well within the range covered by the giant H II regions used as zero point calibrators.

5.3 THE HUBBLE CONSTANT FROM GALAXY CLUSTERS

Any measurement of the Hubble constant within 50–100 Mpc of the Local Group is likely to be affected by important systematic errors due to the existence of large scale bulk motions (Dressler *et al.* 1987). We may use the distance to the Virgo cluster together with the relative distances to rich clusters of galaxies obtained by Dressler *et al.* to quantify the importance of the effect. The distance ratios between several clusters were determined by Dressler *et al.* independently of H_0. Thus, if V_c is the radial velocity of a cluster and D_c its distance, H_0 can be obtained as,

$$H_0=\frac{V_c(D_v/D_c)}{D_v}$$

where D_v is the distance to Virgo. The radial velocities and the distance ratios to Virgo for six rich clusters with redshifts larger than 3000 km s^{-1} are presented in Table 5 together with the values of H_0 obtained using a distance of $D_v=15$ Mpc to Virgo. Assuming that these clusters are at rest relative to the CMWB, we can correct their radial velocities for the motion of the Local Group relative to the CMWB. The relevant projections of this motion, V_{mwb} determined using $V_\odot=614$ km s^{-1} towards $1=269$, $b=28$ (Lubin *et al.* 1985) are given in Table 5. The last column of the table shows the values of H_0 that are obtained after removing V_{mwb} from the cluster radial velocities. Lynden-Bell (1987) has argued that the peculiar motion of the Centaurus cluster relative to the CMWB is due to the gravitational pull of a huge mass concentration located just beyond the Hydra–Centaurus complex. The large value of H_0 for Centaurus may be partly due to this effect and partly due to the gravitational pull of the Perseus cluster on the Local Group. Excluding these two clusters, we obtain a mean value of $H_0=87\pm2$ km s^{-1} Mpc^{-1} for the remaining four clusters in Table 5, which is in remarkably good agreement with the value of $H_0=86\pm7$ km s^{-1} Mpc^{-1} we obtain from H II galaxies (internal consistency errors are quoted). We

Table 5. H_0 from rich clusters.

CLUSTER	V_c	D_c/D_v	V_{mwb}	H_o	H_o^{mwb}
Centaurus	3041	1.7	+523	122	143
Eridanus	4734	3.3	-452	96	87
Perseus	5344	4.5	-319	77	74
A194	5498	3.8	-405	97	90
Coma	6922	5.5	+272	87	83
Klemola 44	8876	6.8	-339	96	87

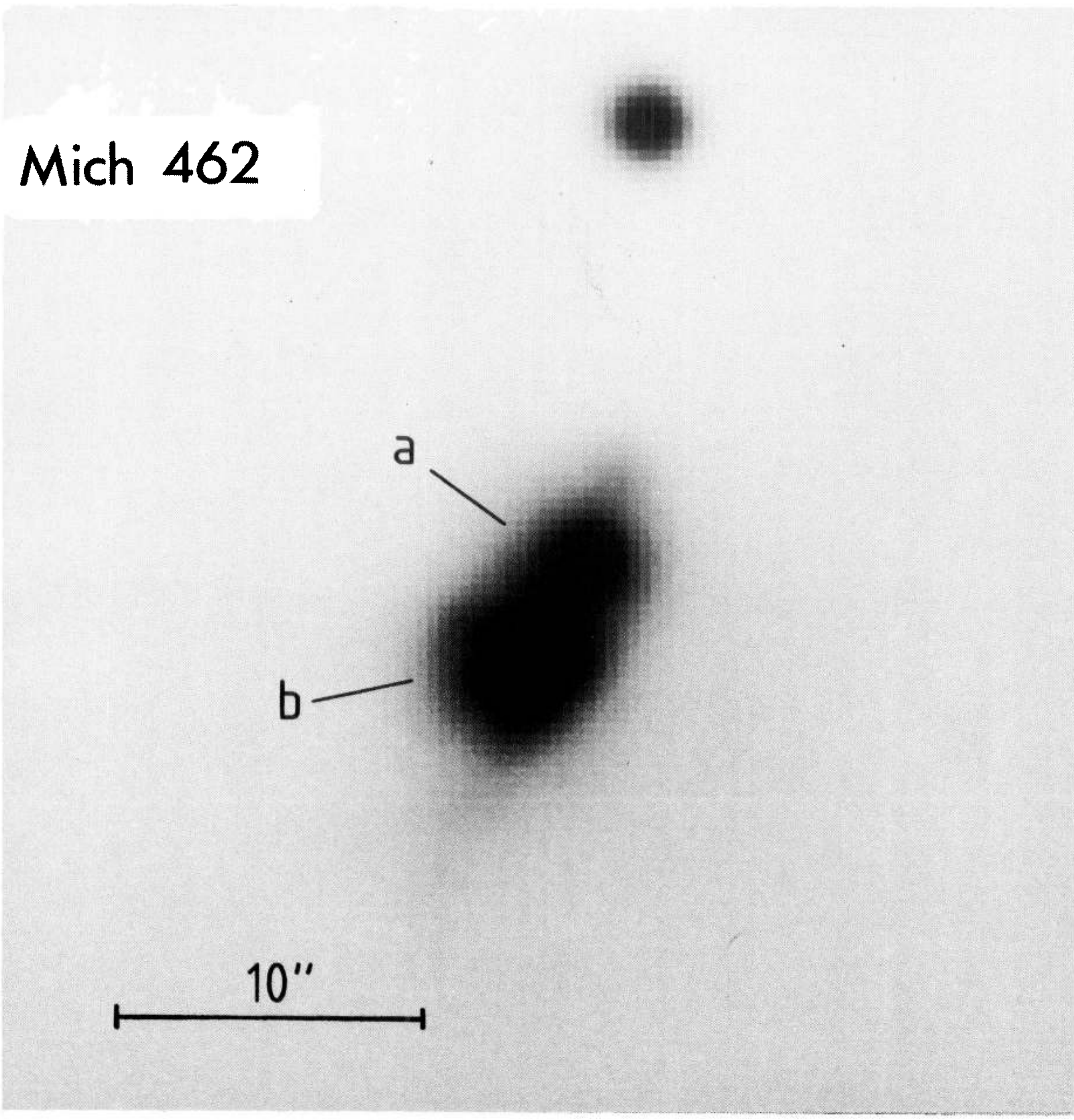

Plate 2. CCD image in blue light of the double H II galaxy SCHG 1150−021 (Mich 462) where the two components are clearly resolved. The echelle spectrum of this galaxy is shown in Fig. 1.

[*facing page* 310]

conclude that galaxies of moderate redshift ($cz<5000\,\mathrm{km\,s^{-1}}$) can be used to measure the Hubble constant *provided they lie at large angular distances from the direction defined by the microwave background dipole.*

6 Discussion

Since there is very little overlap in luminosity and velocity dispersion between giant H II regions and H II galaxies, we must worry about possible systematic differences between the two classes of objects that could bias our distance estimates towards lower values. There are two possible (related) effects that must be considered: zero point errors and curvature of the [$\log L(\mathrm{H}\beta), \log\sigma$] relation. An underestimate of the zero point calibration may arise if many H II galaxies consist of more than one giant H II region superimposed along the line of sight. In fact a surprisingly large fraction of H II galaxies show complex morphology (Melnick 1987). This is illustrated in Plate 1, where we show the echellogram of the double galaxy SCHG 1150−021 (Mich 462), and in Plate 2 where we reproduce a direct CCD image of this galaxy. The two components of this and most other double galaxies in the echelle sample are clearly resolved. In fact, in the case of SCHG 1150−0211 both components are in the sample (Table 1). In other cases, the equivalent widths were too low or the second component too faint to be included in the present study. From deep high resolution CCD imagery and from long-slit spectroscopy we find no evidence for a significant incidence of *unresolved* multiple objects in our sample. Of course if all H II galaxies consist of several components of the same radial velocity exactly superposed on the line of sight we would systematically underestimate their distances without finding any observational evidence of multiplicity! We conclude that, although at high redshifts this may be a serious difficulty, the influence of multiplicity in our present sample does not introduce serious systematic effects.

Curvature of the $\log L(\mathrm{H}\beta)-\log M_z$ relation is the second potentially serious problem we must worry about. The broadening of the emission lines may be affected by the gravity of the overall galaxy. If present, this effect will saturate the [$L(\mathrm{H}\beta), \sigma$] relation at high luminosities where the line broadening will be dominated by the gravity of the old stellar component. However, excluding the two galaxies with $\sigma>60\,\mathrm{km\,s^{-1}}$, where this effect is clearly present, the correlation between $L(\mathrm{H}\beta)$, σ and O/H, for H II galaxies has the same functional form and the same scatter as the correlation for giant H II regions. This strongly suggests that any broadening of the lines by a source not related to the young stellar population must be small. In fact, by imposing the condition that $W(\mathrm{H}\beta)>30$ Å in our sample, we effectively eliminated galaxies where the light of the young component is severely affected by the underlying stellar population. The functional dependence of $L(\mathrm{H}\beta)$ on σ and of R_c on σ support the conclusion that the young components of H II galaxies are gravitationally bound and that gravity is the main source of line broadening in these systems (Terlevich & Melnick 1981; Paper I) although the validity of the relation between R_c and σ for H II galaxies must be confirmed. We conclude, therefore, that our present results are not seriously influenced by systematic differences between H II galaxies and giant H II regions. The effects of multiplicity and interaction with the parent galaxies, however, are clearly important. Thus, although H II galaxies can be observed out to very large redshifts, these effects may limit the applicability of H II galaxies in cosmology to relatively small distances.

7 Conclusions

The main results of the present investigation are the following:

(i) The Hβ luminosities of H II galaxies can be inferred with an accuracy comparable to the observational errors from the widths of their emission lines and their oxygen abundances. Moreover, the correlation between $L(\mathrm{H}\beta)$, σ and O/H for H II galaxies has the same functional dependence and the same scatter as the correlation exhibited by giant H II regions in nearby late-type galaxies.

(ii) Combining giant H II regions and H II galaxies, a value of $H_0=89\pm10\,\mathrm{km\,s^{-1}\,Mpc^{-1}}$ (including zero point errors) is obtained for the Hubble constant after correction for Malmquist bias and for the motion of the Local Group relative to the Cosmic Microwave Background.

(iii) Systematic differences between H II galaxies and giant H II regions related to the properties of the parent galaxies do not appear to be very serious for the present sample but may limit the application of the results to relatively nearby galaxies ($z<0.1$).

(iv) We have obtained a distance of 15 ± 2 Mpc to the Virgo cluster which is largely free of most of the systematic errors which may affect the method because it is obtained using H II galaxies of luminosities comparable to those of the nearby giant H II regions used as zero point calibrators.

(v) A value of $H_0=87\pm10\,\mathrm{km\,s^{-1}\,Mpc^{-1}}$ (including zero point errors) is obtained using distant clusters. The agreement between this value and that obtained using H II galaxies indicates that outside the ridge defined by the Centaurus, Virgo and Perseus clusters, and beyond $3000\,\mathrm{km\,s^{-1}}$ the Hubble flow is reasonably smooth. Close to the ridge, however, the Hubble flow appears to be seriously perturbed by large-scale peculiar motions for galaxies out to $cz\sim10\,000\,\mathrm{km\,s^{-1}}$.

Acknowledgments

It is a pleasure to thank the mountain staff at La Silla, Las Campanas and Cerro Tololo for their friendly help during the many observing runs needed to complete the data for this paper. We also thank Jack Baldwin for his help with the echelle and with the reduction programs at the CTIO computing centre. We are grateful to Leon Lucy for advice on the maximum likelihood methods both here and in Paper I. We would like in particular to express our gratitude to Edmond Giraud for his patience in teaching us how to deal with the devilish Malmquist bias. Of course, if we have done it wrong it is all his fault!

References

Aaronson, M., Huchra, J., Mould, J., Schechter, P. L. & Tully, R. B., 1982. *Astrophys. J.*, **258,** 64.
Aaronson, M., Bothun, G., Mould, J., Huchra, J., Schommer, R. A. & Cornell, M. E., 1986. *Astrophys. J.*, **302,** 536.
Bottinelli, L., Gouguenheim, L., Paturel, G. & Teerikorpii, P., 1986. *Astr. Astrophys.*, **156,** 157.
Campbell, A. W., Terlevich, R. & Melnick, J., 1986. *Mon. Not. R. astr. Soc.*, **223,** 811.
Coppetti, M. V. F., Pastoriza, M. A. & Dottori, H. A., 1986. *Astr. Astrophys.*, **152,** 427.
de Vaucouleurs, G. & Peters, W. L., 1986. *Astrophys. J.*, **303,** 19.
Dressler, A., Faber, S. M., Burstein, D., Davies, R. L., Lynden-Bell, D., Terlevich, R. & Wegner, G., 1987. *Astrophys. J.*, **313,** L37.
Fairall, A. P., 1980. *Mon. Not. R. astr. Soc.*, **191,** 391.
Giraud, E., 1987. *Astr. Astrophys.*, **174,** 23.
Haro, G., 1956. *Bull. Ton. Tac.*, **14,** 2, 8.
Hazard, C., 1985. In: *Star Forming Dwarf Galaxies and Related Objects*, p. 456, eds Kunth, D., Thuan, T. X. & Tran Thanh Van, J., Frontières, Paris.
Lubin, P. M., Villela, T., Epstein, G. L. & Smoot, G. F., 1985. *Astrophys. J.*, **298,** L1.
Lynden-Bell, D., 1987. *Q. Jl R. astr. Soc.*, **28,** 187.
Markarian, B. E., 1967. *Astrofizika*, **3,** 55.
Markarian, B. E., Lipovetskii, V. A. & Stepanian, D. A., 1981. *Astrofizika*, **17,** 619.
McAlpine, G. M. & Williams, G. A., 1981. *Astrophys. J. Suppl.*, **45,** 113.
Melnick, J., 1987. In: *Starbursts and Galaxy Evolution*, p. 215, eds Thuan, T. X., Montmerle, T. & Tran Thanh Van, T., Frontières, Paris.
Melnick, J., Terlevich, R. & Eggleton, P. P., 1985. *Mon. Not. R. astr. Soc.*, **216,** 255.
Melnick, J., Moles, M., Terlevich, R. & Garcia-Pelayo, J. M., 1987. *Mon. Not. R. astr. Soc.*, **226,** 849 (Paper I).
Pagel, B. J. E., Terlevich, R. & Melnick, J., 1986. *Publs astr. Soc. Pacif.*, **98,** 1005.

Sandage, A. & Tammann, G. A., 1974. *Astrophys. J.*, **190**, 525 (ST74).

Sandage, A., 1975. In: *Stars and Stellar Systems*, Vol. 9, p. 778, University of Chicago Press.

Sandage, A., 1984. In: *Large-scale Structure of the Universe, Cosmology and Fundamental Physics*, p. 127, eds Setti, G. & Van Hove, L., Garching, ESO.

Sandage, A., 1986. *Astrophys. J.*, **307**, 1.

Sargent, W. L. W. & Searle, L., 1970. *Astrophys. J*, **162**, L155.

Seyfert, K., 1940. *Astrophys. J.*, **91**, 261.

Skillman, E. D., Melnick, J., Terlevich, R. & Moles, M., 1988. *Astr. Astrophys.*, **196**, 31.

Smith, M. G., Aguirre, C. & Zemelman, M., 1976. *Astrophys. J. Suppl.*, **32**, 217.

Tammann, G. A., 1987. *Observational Cosmology, IAU Symp. No. 124*, p. 151, eds Hewitt, A., Burbidge, G. & Fang, L. Z., Reidel, Dordrecht (TA87).

Tammann, G. A. & Sandage, A. R. 1985. *Astrophys. J.*, **294**, 81.

Teerikorpii, P., 1984. *Astr. Astrophys.*, **54**, 661.

Terlevich, R. & Melnick, J., 1981. *Mon. Not. R. astr. Soc.*, **195**, 839.

Yahil, A., Sandage, A. R. & Tammann, G. A., 1977. *Astrophys. J.*, **217**, 903.

Zwicky, F., 1966. *Astrophys. J.*, **143**, 192.

Zwicky, F., 1971. *Catalogue of Selected Compact Galaxies and Post-eruptive Galaxies*, published by the author, Switzerland.